IEEE Access
Multidisciplinary | Rapid Review | Open Access Journal

Received 13 September 2022, accepted 4 October 2022, date of publication 10 October 2022, date of current version 14 October 2022.

Digital Object Identifier 10.1109/ACCESS.2022.3213046

RESEARCH ARTICLE

Research on Equalization Strategy Based on Credibility Factor Inference for Lithium-Ion Battery Packs

LI LIAO, HENG CHEN, SHU SUN, HONGGUANG LI, JIUCHUN JIANG, (Senior Member, IEEE), AND TIEZHOU WU

Hubei Key Laboratory for High-Efficiency Utilization of Solar Energy and Operation Control of Energy Storage System, Hubei University of Technology, Wuhan 430068, China

Corresponding author: Heng Chen (chenheng1023@163.com)

This work was supported in part by the National Natural Science Foundation of China under Grant 52177212, and in part by the Science and Technology Research Program of Hubei Provincial Department of Education under Grant T2021005.

ABSTRACT In this paper, a two-stage equalization topology based on Zero-Voltage Switching Quasi-Resonant Converter (ZVS QRC) is proposed to solve the problems of long equalization time and low energy utilization of series lithium-ion battery packs. The equalization topology is divided into two forms: intra-group and inter-group, ZVS QRCs are adopted in both intra-group and inter-group, which can equalize any single cell within a group, and the equalization circuit within each pack can equalize simultaneously, which greatly reduces the equalization time, and reduces the switching loss during the equalization process by introducing quasi-resonant circuit to improve the energy utilization. Taking the State of Charge (SOC) as the equalization target, a group equalization strategy based on the Credibility Factor (C-F) inference model is proposed. The strategy defines the SOC unbalance degree of a single battery, gets the group unbalance degree according to the C-F inference model, and gets the group equalization state from the unbalance degree, to control the group for equalization. Matlab/Simulink software is used to build the model and simulate it. The experimental results demonstrate that the proposed topology saves approximately 25% of the equalization time compared to the traditional Buck-Boost group equalization topology. Under the same static and charge/discharge conditions, the equalization time is reduced by about 21% and the energy utilization is improved by about 6% after using the C-F inference model for equalization compared to the fixed-threshold method.

INDEX TERMS Credibility factor, battery equalization, zero-voltage switching, quasi-resonance, SOC.

I. INTRODUCTION

Lithium-ion batteries are widely used in electric vehicles because of their high power and energy density, long life, and low self-discharge rate [1], [2], [3]. Multiple batteries need to be connected in series to meet the power and capacity requirements of electric vehicles. However, the inconsistency of battery capacity, voltage, and internal resistance due to the variation of the internal resistance, unequal capacity, and aging will affect the performance and service life of the battery pack [4], [5], [6]. Therefore, it is necessary to study the battery equalization technology to reduce the inconsistency of the battery pack and prolong the service life of the battery pack.

Equilibrium methods can be divided into passive and active [7], [8], [9]. Passive equalization [10] dissipates the excess energy through parallel resistors, which is simple and low cost to control, but it has problems such as high losses and significant temperature rise during equalization. Active equalization [11], [12], [13], [14] uses inductors, capacitors, and converters to achieve inter-cell energy transfer. Vardhan et al. presented in [15] an inductor-based equalization topology, but

The associate editor coordinating the review of this manuscript and approving it for publication was Zhiwei Gao.

the topology uses more switches and has higher energy losses. Fan et al. presented in [16] an improved Buck-Boost circuit topology, but it can only achieve energy transfer between two adjacent batteries, with low equalization efficiency and slow equalization speed. Ma et al. presented in [17] a two-stage equalization topology based on the Buck-Boost circuit, which effectively improves the consistency of the battery pack, but the equalization efficiency is not high and the switching losses are large.

The equalization topologies have been improved in [15], [16], and [17], but none of them considered the loss of switching tubes during the equalization process. Resonant circuits have been introduced into the equalization topology in [18] and [19], which effectively improved the equalization efficiency, but there are also problems of complex control, long equalization time, and high cost.

Considering the advantages and disadvantages of the above topologies, a two-stage equalization topology based on ZVS QRC is proposed in this paper, which groups the cells, allows the equalization between any single cell within the group, and can be equalized simultaneously, and reduces the switching losses by introducing quasi-resonant circuits. Thus, it show better advantages in both equalization speed and energy utilization.

In addition to the equalization topology, the battery equalization technology also includes the equalization strategy. According to the judgment basis, the equalization strategy can be divided into the equalization strategy based on terminal voltage consistency, the equalization strategy based on capacity consistency and the equalization strategy based on SOC consistency. References [20], [21], [22], and [23] uses terminal voltage as the equalization criterion, but the terminal voltage is influenced by the operating conditions and other factors, and the battery pack is prone to transfer the energy from the low-capacity and high-voltage single cell to the high-capacity and low-voltage single cell during the cyclic charging and discharging plateau period, which further increases the capacity inconsistency. When the battery pack works in the plateau period, its voltage changes more slowly with time, which makes it difficult to accurately judge the equalization of the battery pack, and it is somewhat blind to use voltage as the equalization target. References [24], [25], and [26] used capacity as the equalization criterion, however, considering that the battery pack is charged and discharged with the cut-off voltage as the cut-off condition, the difference between the actual maximum remaining capacity and charging and discharging rate of each single cell in operation makes the capacity and voltage of the single cell inconsistent. The single cell with high remaining capacity may have reached the cut-off voltage, which may cause overcharging if it continues charging. Meanwhile, if there are more cells in the battery pack, it is difficult to ensure the accuracy of online capacity estimation. SOC is a cumulative quantity of time and has a more stable relationship with the open-circuit voltage. And it has a high resolution in the voltage plateau period, which can better complete the equalization judgment in the voltage plateau period [27], [28].

To better reflect the consistency of battery pack, taking the SOC as the equalization target, an equalization strategy based on the C-F inference model is proposed in this paper. The strategy defines the unbalance degree of the single cell and the battery pack, and use the C-F inference model to judge the battery pack inconsistency and provide the criterion to achieve the equalization, in order to reduce the battery pack inconsistency and improve the battery pack energy utilization.

The main contributions of this paper are as follows:

1) A two-stage balanced topology based on the ZVS QRC is proposed, and the advantages of the topology are further analyzed.
2) The equalization control strategy based on the C-F inference model is proposed and compared with the fixed-threshold method to verify the superiority of the strategy.
3) To better quantify the equalization effect, the energy utilization rate is defined for evaluation.

The structural arrangement of this paper is as follows. The second section introduces the topology of two-stage equalization based on the ZVS QRC and analyses its working principle. The third section introduces the control strategy based on the C-F inference model. In the fourth section, the equilibrium topology and the control strategy based on the C-F inference model are verified by modeling and simulation with Matlab/Simulink software. Finally, the relevant conclusions are given in the fifth section.

II. GUIDELINES FOR MANUSCRIPT PREPARATION

A. ABBREVIATIONS AND ACRONYMS

The traditional Buck-Boost equalization topology is shown in Fig. 1, containing m single cells, 2m-2 MOSFE, 2m-2 diodes, and m-1 inductors. When the batteries are being equalized, the energy is transferred through the inductors and the control is relatively simple, but when the number of batteries is large, the equalization time is slow, and there are more switching tubes in the circuit, and the turn-on loss of the switching tubes increases as the number of switches increases.

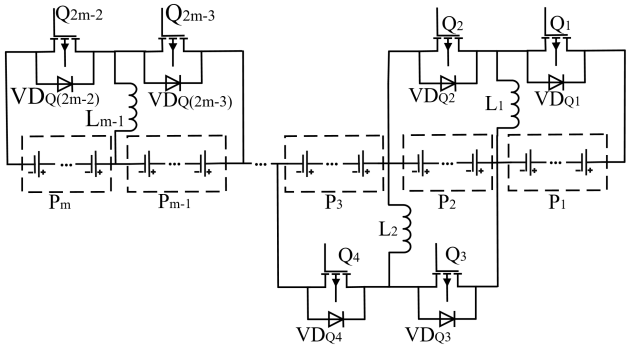

FIGURE 1. Traditional buck-boost balanced topology.

To address the problems of the above traditional topology, a two-stage equalization topology based on ZVS QRC is proposed in this paper, and its topological framework is shown in Fig. 2. The n single cells are grouped, and there are m cell groups, each group contains p single cells. Each cell group contains one intra-group equalization subcircuit, that is, there are m intra-group equalization subcircuits; there are m-1 inter-group equalization circuits. Both the intra-group equalization subcircuit and the inter-group equalization circuit use zero-switching quasi-resonant circuits. The following is an example of an inter-group equalization subcircuit.

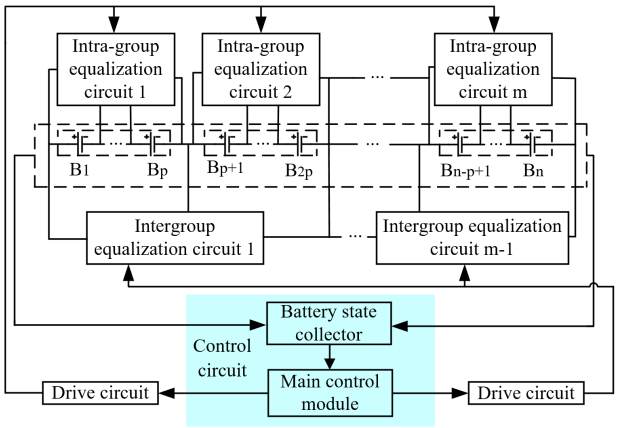

FIGURE 2. Two-stage balanced topology framework diagram.

The intra-group equalization subcircuit contains p single cells, 2p double-layer switches (including upper switches and lower switches), and ZVS QRC. P double-layer switches are connected to the positive and negative terminals of each cell, respectively. The ZVS QRC consists of two inductors L and L_r, one capacitor C_r, one switch tube (MOSFET) S_a, and two diodes D_1 and D_2. The equilibrium topology based on ZVS QRC is shown in Fig. 3.

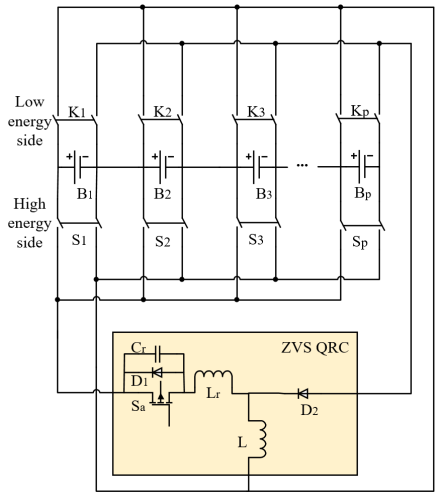

FIGURE 3. Equalization topology based on ZVS QRC.

This equalization topology has the following three advantages:

1) The circuit topology can achieve energy transfer between any cells by selecting the switch on/off, thus shortening the energy transfer path and reducing the equalization time.
2) The equalization topology adopts ZVS QRC, which can effectively reduce the turn-on loss of the switching tubes and improve the equalization efficiency.
3) The equalization topology uses common switches instead of MOSFET tubes, which is simple to control and less costly.

B. PRINCIPLE OF THE EQUALIZATION CIRCUIT

In this subsection, the equalization topology will be analyzed. Assuming that single cell B_1 has the highest energy and single cell B_2 has the lowest energy, the energy transfer process will be carried out in single cell B_1 and B_2, and its energy transfer process is divided into two main stages. The energy transfer path is shown in Fig. 4.

Stage 1: the lower switch S_1 on the high energy side of the equalization topology closes and the switch tube S_a conducts, and the single cell B_1, the lower switch S_1, the switch tube S_a, the inductor L_r and L form the B_1 discharge circuit. The energy of the single cell B_1 is transferred to the inductor L. Since the value of resonant inductor L_r is much smaller than the value of inductor L, L_r is ignored in the analysis for convenience. the discharge circuit is shown in Fig. 4 a).

Assuming that the switching tube S_a conduction resistance is R_1 during discharge, the circuit equation of the discharge circuit is:

$$L\frac{di_{L1}}{dt} + i_{L1}R_1 = V_{B1} \tag{1}$$

where i_{L1} is the current flowing through the inductance L, V_{B1} is the terminal voltage of cell B_1.

The current of inductor L can be calculated from (1).

$$i_{L1} = i_0 e^{-\frac{R_1 t}{L}} + \frac{V_{B1}}{R_1}(1 - e^{-\frac{R_1 t}{L}})(0 < t < t_{on}) \tag{2}$$

where i_0 is the initial current of the inductor L, and t_{on} is the conduction time of switching tube S_a.

The maximum value of the current of the inductor L is:

$$i_{L1\max} = i_0 e^{-\frac{R_1 t_{on}}{L}} + \frac{V_{B1}}{R_1}(1 - e^{-\frac{R_1 t_{on}}{L}}) \tag{3}$$

Stage 2: When switch S_a is off, the upper switch K_2 on the low energy side turn off and diode D_2 conducts. Single cell B_2, upper switch K_2, diode D_2, and inductor L form the B2 charging circuit. The energy in the inductor L is transferred to the single cell B_2.

Assuming that the internal resistance of the diode and inductor L in the circuit is R_2, the circuit equation of the B_2 charging circuit is:

$$L\frac{di_{L2}}{dt} + i_{L2}R_2 + V_{B2} + V_D = 0 \tag{4}$$

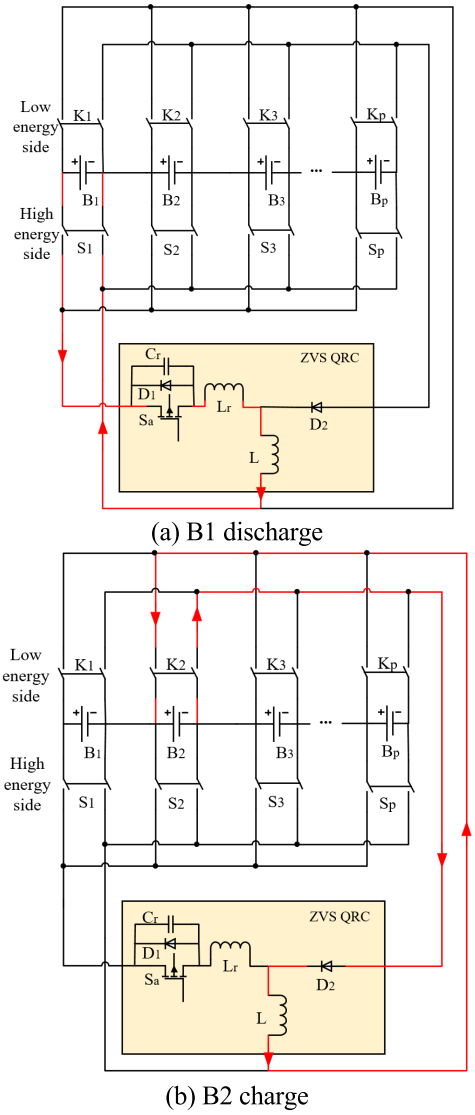

FIGURE 4. Energy transfer path of cell B1 and cell B2.

where V_{B2} is the terminal voltage of the single cell B_2, V_D is the tube voltage drop of the diode, and i_{L2} is the current of the inductor L.

From (4), the current of the inductor L during the charging of the single cell B_2 can be calculated as:

$$i_{L2} = i_{L1\max} e^{-(t-t_{on})\frac{R_2}{L}} - \frac{V_{B2}+V_D}{R_2}(1-e^{-(t-t_{on})\frac{R_2}{L}}) \quad (5)$$

C. CONDUCTION PRINCIPLE OF ZVS

The switching circuit operates on a repetitive switching cycle, and any moment in the switching cycle can be selected as the starting point for analysis. Choosing a suitable starting point simplifies the analysis process. Therefore, in this paper, the switching tube S_a off moment is chosen as the starting point for analysis.

During S_a turn-off, capacitor C_r and inductor L_r are introduced to put the circuit in a resonant state. Using the energy conversion of the inductor and capacitor to each other, the voltage drops to 0 before the switch turns on, eliminating the voltage and current overlap during the turn-on process and thus eliminating the turn-on loss. The waveform diagram of ZVS QRC is shown in Fig. 5.

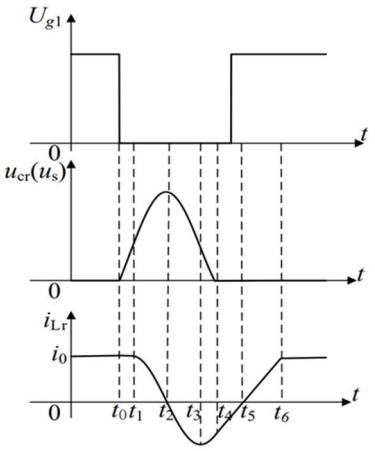

FIGURE 5. Waveform diagram of ZVS QRC.

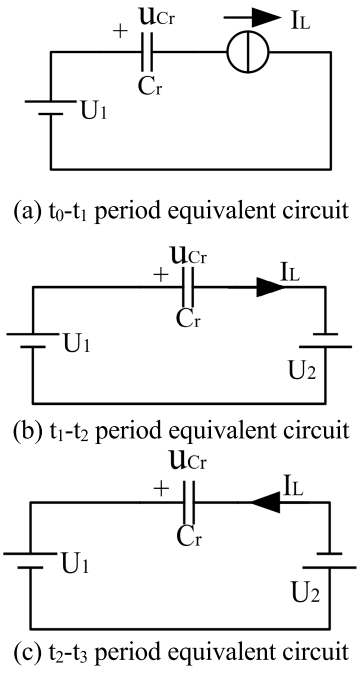

FIGURE 6. Equivalent circuit of ZVS QRC.

Before the moment t_0, the switch S_a is on and the diode D_1 is in the cutoff state, $u_{cr} = 0$, $i_{Lr} = i_L$; at the moment t_0, Sa is off and the inductor L and L_r charge C_r. It can be equated to a current source since the inductor L is large. u_{cr} rises linearly. Until the moment t_1, the capacitor C_r voltage is equal to $U_1 + U_2$. where U_2 is the terminal voltage of the inductor L. The equivalent circuit for the t_0-t_1 time period is

shown in Fig. 6 a), and the rate of rising during this phase is:

$$\frac{du_{cr}}{dt} = \frac{i_L}{C_r} \tag{6}$$

At the moment t_1, diode D_2 starts to conduct, the inductor L is renewed by diode D_2. C_r, L_r, U_1, and U_2 form a resonant circuit. In the resonance process, L_r charges C_r, u_{cr} rises and i_{Lr} falls, and at the moment t_2, i_{Lr} falls to 0 and u_{cr} reaches the resonance peak. t_1-t_2 time period equivalent circuit is shown in Fig.6 b).

After the moment t_2, C_r charges L_r, i_{Lr} changes direction, u_{cr} decreases continuously, and at the moment t_3, the voltage across the inductor L_r is 0 and i_{Lr} reaches the reverse resonance peak. The t_2-t_3 period equivalent circuit is shown in Fig. 6 c).

After the moment t_3, L_r charges C_r in reverse and u_{cr} continues to fall. At the moment t_4, $u_{cr} = 0$.

The equation of the circuit resonance process at moments t_1-t_4 is:

$$\begin{cases} L_r \frac{di_{Lr}}{dt} + u_{cr} = U_1 + U_2 \\ C_r \frac{du_{cr}}{dt} = i_{Lr} \\ u_{cr|t=t_1} = U_1 + U_2, \quad i_{Lr|t=t_1} = i_0, \quad t \in [t_1, t_4] \end{cases} \tag{7}$$

By solving (7), we can obtain u_{cr}:

$$u_{Cr(t)} = \sqrt{\frac{L_r}{C_r}} i_L \sin w_r(t - t_1) + U_1 + U_2, \quad t \in (t_1, t_4) \tag{8}$$

$$w_r = \frac{1}{\sqrt{L_r C_r}}, \quad t \in (t_1, t_4) \tag{9}$$

At t_4-t_5, u_{cr} is clamped at 0 and the voltage across the inductor is $U_1 + U_2$, and i_{Lr} linearly decays to 0. Since the voltage across the switch S_a is 0 during this time, the control switch S_a conducts during this period and no turn-on loss is generated.

At moments t_5-t_6, S_a conducts and i_{Lr} rises linearly. At moment t_6, $i_{Lr} = i_L$, the resonance process ends.

According to (8) and (9), to achieve zero-voltage turn-on of the switch Sa, it is necessary to satisfy that u_{cr} is 0 during the resonance process, that is:

$$\sqrt{\frac{L_r}{C_r}} i_L > U_1 + U_2 \tag{10}$$

D. IMPACT OF THE INTRODUCTION OF ZVS QRC

In the absence of the introduction of a quasi-resonant circuit, the capacity reduction of B_1 and the capacity increase of B_2 during the discharge of the single cell B_1 are:

$$\Delta C_{B1} = \int_0^{DT} i_{L1} dt = \frac{i_0 L}{R_1}\left(1 - e^{\frac{R_1}{L}DT}\right) + \frac{U_1}{R_1}\left(DT - \frac{L}{R_1} + \frac{L}{R_1} e^{\frac{R_1}{L}DT}\right) \tag{11}$$

$$\Delta C_{B2} = \int_{DT}^{T} i_{L2} dt = \left(i_0 e^{-\frac{R_2}{L}DT} + \frac{U_1}{L}DT\right)(1 - D)T \tag{12}$$

With the introduction of the quasi-resonant circuit, the charging current of the single cell B_2 is:

$$i_{B2} = i_{L2} - i_{Lr} \tag{13}$$

Therefore, the capacity reduction of the single cell B_1 and the capacity increase of B_2 after the introduction of the quasi-resonant circuit are:

$$\Delta C'_{B1} = \int_0^{DT} i_{L1} dt + \int_{t_0}^{t_6} i_{Lr} dt = \Delta C_{B1} + \frac{i_0 L_r}{U_1 + U_2}\left(1 - \cos\left(\frac{U_1 + U_2}{i_0}\right)\sqrt{\frac{C_r}{L_r}}\right) \tag{14}$$

$$\Delta C'_{B2} = \int_{DT}^{T} i_{B2} dt \approx 2\pi\sqrt{L_r C_r} \tag{15}$$

The relationship between SOC and the capacity of a single cell is

$$\Delta SOC = \frac{\Delta C}{C} \tag{16}$$

where C is the capacity of the single cell.

From (11) and (16), it can be seen that the SOC reduction of single cell B_1 is increased by the introduction of the quasi-resonant circuit compared to the non-introduction of the quasi-resonant circuit. The SOC increment is the switching loss eliminated by the introduction of L_r and C_r, which will be transferred from cell B_1 to cell B_2 during the equalization process. So the SOC increment during the charging of cell B_2 is larger compared to that without the introduction of the quasi-resonant circuit. Thus it can be seen that the topology proposed in this paper helps to improve the capacity utilization.

From the analysis in this section, it can be seen that the ZVS used in this paper can not only realize the energy transfer of the battery pack through inductor L, L_r, and capacitor C_r, but also the introduction of inductor L_r and capacitor C_r can reduce the turn-on loss of the switching tube and improve the energy utilization of the battery pack.

III. EQUILIBRIUM STRATEGY BASED ON C-F INFERENCE

A. UNBALANCED CREDIBILITY

The current equalization variables are mainly voltage, SOC, and remaining capacity. Taking the voltage as the equalization variable, only the voltage acquisition module needs to be used for detection, which does not require a lot of calculations, but when the battery capacity is between 10% and 90%, the battery voltage changes very little and the equalization effect depends largely on the acquisition accuracy of the voltage acquisition module. Taking the remaining capacity as the equalization variable, the energy utilization of all cells in the battery pack can be maximized. But the battery capacity can only be obtained in the static state, and the problems of accuracy and real-time estimation of the remaining capacity

cannot be solved. Therefore, it can only be done offline at present, and it is difficult to guarantee the estimation accuracy. Battery SOC is a comprehensive characterization of the battery voltage, internal resistance, and other parameters. Using battery SOC as the equalization variable can essentially improve the inconsistency of the battery and avoid the impact of the difference in maximum available capacity, thus enhancing the battery life and improving the battery efficiency.

In this paper, a new equilibrium index is proposed with the battery SOC as the equilibrium target: the unbalance credibility. Firstly, the unbalance credibility of a single cell is calculated based on its SOC to determine the equilibrium state of a single cell, and then the unbalance credibility of the battery pack is inferenced through the C-F model to determine the equilibrium state of the battery pack. The flow of the credibility inferred for the equalization topology is shown in Fig. 7.

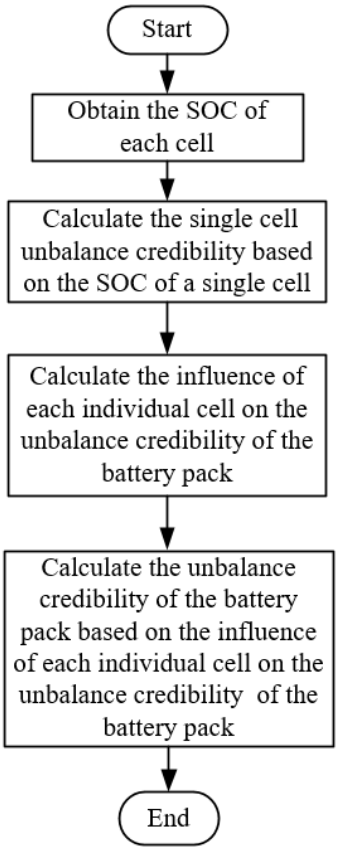

FIGURE 7. The flow of credibility inferred for equalization topology.

B. UNBALANCE CREDIBILITY OF SINGLE CELL

With SOC as the equalization target, the equalization operation is usually performed for cells whose SOC is outside the threshold range [$SOC_{avg} - \Delta SOC$, $SOC_{avg} + \Delta SOC$]. The equalization threshold ΔSOC directly affects the equalization state of the cell, and ΔSOC is usually taken to be 2%-4% in engineering applications. Therefore, in this paper, we take $SOC_{min} = 2\%$, $SOC_{max} = 4\%$ and define the single cell unbalance credibility base on SOC as:

$$F_{BS,i} = \begin{cases} 0.5(\varphi - 2) & 0 \le \varphi \le 4 \\ 1 & \varphi > 4 \end{cases} \tag{17}$$

where φ is the absolute value of the difference between the SOC of single cell i and the average SOC of the battery pack.

From (17), the range of $F_{BS,i}$ is [−1,1], and it is stipulated that: the larger the single cell unbalance credibility $F_{BS,i}$, the higher the credibility that the single cell is in unbalance; the smaller the $F_{BS,i}$, the lower the credibility that the single cell is in unbalance; when $F_{BS,i} = 0$, it is stipulated that the single cell i is in the equilibrium state, that is:

$$\begin{cases} F_{BS,i} > 0, & \text{In an unbalanced state} \\ F_{BS,i} \le 0, & \text{In balanced state} \end{cases} \tag{18}$$

C. UNBALANCE CREDIBILITY OF BATTERY PACK

The unbalance credibility of the battery pack is jointly determined by the unbalance credibility of each cell in the battery pack, which can directly reflect the discrete degree of the energy state of the battery pack. $F_{S,i}$ is the influence of single cell i on the unbalance credibility of the battery pack, and the definition of $F_{S,i}$ is as follows:

$$F_{S,i} = \begin{cases} -\dfrac{|SOC_i - SOC_{avg}|}{\sum_{j=1}^{q1} |SOC_{avg} - SOC_j|} & |SOC_{avg} - SOC_i| \le \varepsilon \\ \dfrac{|SOC_i - SOC_{avg}|}{\sum_{j=1}^{q2} |SOC_{avg} - SOC_j|} & |SOC_{avg} - SOC_i| > \varepsilon \end{cases} \tag{19}$$

$$\varepsilon = \frac{\sum_{j=1}^{n} |SOC_{avg} - SOC_j|}{n} \tag{20}$$

In (19) and (20), SOC_j is the *SOC* of single cell j; q_1 is the number of single cells in the battery satisfying $|SOC_{avg} - SOC_i| < \varepsilon$, q_2 is the number of single cells in the battery satisfying $|SOC_{avg} - SOC_i| > \varepsilon$, and ε is the discrete of the battery.

According to the uncertainty reasoning of the C-F model, the unbalance credibility of the battery pack derived from a single cell can be obtained as $F^o_{S,i} = F_{S,i} \cdot \max(0, F_{BS,i})$. The combined unbalance credibility derived from two single cells in the battery pack is $F^o_{S,i1} \otimes F^o_{S,i2}$. Its operation is divided into 3 cases.

1) When $F^o_{S,i1} > 0$ and $F^o_{S,i2} > 0$, the combined unbalance credibility of the two single cells is $F^o_{S,i1} \otimes F^o_{S,i1} = F^o_{S,i1} + F^o_{S,i2} - F^o_{S,i2} * F^o_{S,i2}$.
2) When $F^o_{S,i1} < 0$ and $F^o_{S,i2} > 0$, the combined unbalance credibility of the two single cells is $F^o_{S,i1} \otimes F^o_{S,i2} = F^o_{S,i1} + F^o_{S,i2} + F^o_{S,i2} * F^o_{S,i2}$.
3) When $F^o_{S,i1} * F^o_{S,i2} < 0$, the combined unbalance credibility of the two single cells is $F^o_{S,i1} \otimes F^o_{S,i2} = \frac{F^o_{S,i1} + F^o_{S,i2}}{1 - min(|F^o_{S,i1}|, |F^o_{S,i2}|)}$.

When there are more than 3 single cells in the battery pack in the unbalanced state, the unbalanced credibility of the battery pack can be calculated according to the above 3 cases in a two-by-two composite, and the unbalanced credibility of the battery pack based on SOC is $F^o_S = F^o_{S,i1} \otimes F^o_{S,i2} \otimes \ldots \otimes F^o_{S,in}$.

D. EQUALIZATION CONTROL STRATEGY

In this paper, an equalization strategy based on C-F inference is proposed to reduce the discrete degree of battery SOC. In subsection B, the unbalance credibility is first introduced to convert the cell SOC into a numerical quantity to represent the discrete degree of SOC, then the unbalance credibility $F_{BS,i}$ of a single cell based on SOC is calculated and finally the equalization status of a single cell is judged based on $F_{BS,i}$.

In subsection C, the influence of the unbalance credibility of a single cell on the unbalance credibility of a battery pack $F_{S,i}$ is first calculated, and then the unbalance credibility of a battery group F^o_S is inferred and calculated. When the unbalance credibility of the battery group F^o_S is greater than the critical value F^o_{th}, then it can be determined that the battery group is in imbalanced state. To improve energy utilization, the equalization control strategy of intra-group equalization first and then inter-group equalization will be adopted in this paper. The equalization flow chart is shown in Fig. 8.

IV. ANALYSIS OF SIMULATION RESULTS

In this paper, Matlab/Simulink 2019b is used to model and simulate the equalization topology. The parameters of the lithium-ion batteries are 3.7V/2.5Ah, and the initial SOC values of the 12 single cells in the battery pack are 81%, 76%, 73%, 71%, 68%, 64%, 62%, 60%, 58%, 57%, 54%, 52%; The equalization simulation model includes battery modules, oscilloscopes, double-layer switches, switch control modules and C-F inference calculation modules. Oscilloscopes are used to collect the SOC value of each single cell; Switch control modules are used to turn on and off the double-layer switch according to the state of each single cell in the battery pack; C-F inference calculation modules mainly consist of Matlab function, which the main function is to calculate the unbalance credibility of each single cell and the whole battery pack. To verify the performance of the proposed topology and algorithm, the following experiments are conducted to compare the proposed topology with the traditional topology and the C-F inference with the fixed-threshold method, respectively.

In the equalization circuit, the equalization topology and control strategy can have an impact on the equalization efficiency due to the conduction loss caused by the internal resistance of the battery, the diode on-resistance, and the switching loss of the MOSFET. The efficiency when the battery is in static, charging and discharging states is analyzed in (21).

(1) When the battery pack is in charge, the efficiency of the battery pack can be expressed as the ratio of the sum of the energy absorbed by all cells to the energy supplied by the external power source.

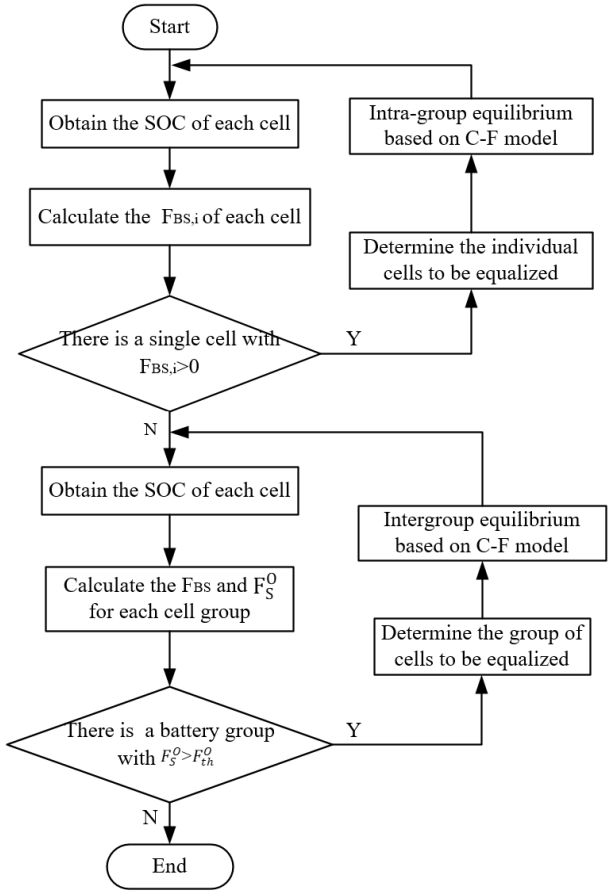

FIGURE 8. Equalization control flow chart.

(2) When the battery pack is in discharge, the efficiency of the pack can be expressed as the ratio of the energy absorbed by the external load to the energy supplied by the battery pack.

(3) When the battery pack is in the static state, the efficiency of the battery pack equalization is expressed as the ratio of the sum of energy absorbed by the low-energy cells to the sum of energy released by the high-energy cells.

Energy utilization η is adopted to quantify the equalization effect of the battery pack in this paper, the η as shown in (21).

$$\eta = \begin{cases} \dfrac{(\sum SOC_{aft} - \sum SOC_{bef})^* C}{n \int I(t)dt}, & \text{in the charging state} \\ \left| \dfrac{n \int I(t)dt}{(\sum SOC_{aft} - \sum SOC_{bef})^* C} \right|, & \text{in the discharged state} \\ \dfrac{\sum SOC_{1aft} - \sum SOC_{1bef}}{\sum SOC_{2aft} - \sum SOC_{2bef}}, & \text{in the static state} \end{cases} \tag{21}$$

where SOC_{bef} and SOC_{aft} are the sum of SOC of all cells in the battery pack before and after equalization, respectively. SOC_{1bef} and SOC_{1aft} are the sum of SOC of low-energy cells in the battery pack before and after equalization, respectively. SOC_{2bef} and SOC_{2aft} are the sum of SOC of high-energy cells in the battery pack before and after equalization, respectively. I(t) is the charging/discharging current of the battery pack at

time t. I(t) is positive when charging, and I(t) is negative when discharging; n is the number of cells in the battery pack, and C is the capacity of the battery.

A. PERFORMANCE VERIFICATION OF TOPOLOGY

To verify the equalization performance of the two-stage equalization topology based on the ZVS QRC proposed in this paper, comparison experiments with the conventional Buck-Boost group equalization topology are conducted. The comparison experiments use the fixed threshold method, and the variation of SOC of each single cell is shown in Fig. 9 a) and Fig. 9 b), respectively.

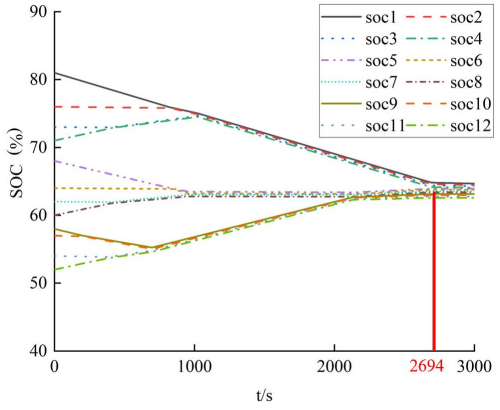

(a) Traditional Buck-Boost grouping topology

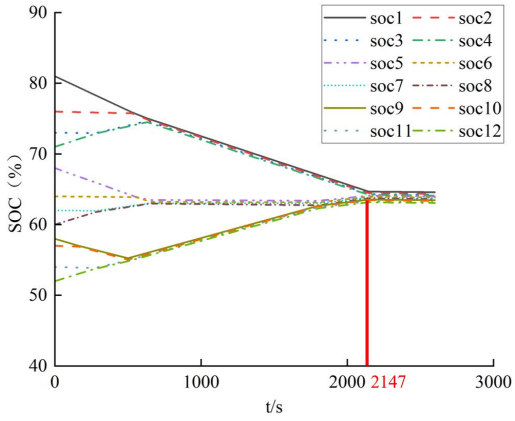

(b) The ZVS QRC proposed in this paper

FIGURE 9. Variation in SOC of each single cell.

As shown in Fig. 9, the traditional Buck-Boost group equalization topology takes about 2694 s to complete equalization in the static state, while the equalization topology proposed in this paper takes only 2147 s to complete equalization, which reduces the equalization time by about 25.48%. Therefore, the equalization topology proposed in this paper can improve the equalization speed.

After equalization, the SOC of each single cell are shown in Table 1.

From Table 1, it can be seen that the extreme difference of the battery pack is reduced from 29% to 2.25% by using

TABLE 1. SOC of each single cell before and after equalization.

Number	Initial SOC	Traditional Topology	Topology proposed in this paper
B1	81%	64.81%	64.67%
B2	76%	64.56%	64.45%
B3	73%	64.39%	64.32%
B4	71%	64.14%	64.21%
B5	68%	63.92%	64.08%
B6	64%	63.75%	63.95%
B7	62%	63.55%	63.84%
B8	60%	63.40%	63.71%
B9	58%	63.14%	63.59%
B10	57%	62.96%	63.48%
B11	54%	62.78%	63.32%
B12	52%	62.56%	63.21%
Mean Value	64.67%	63.66%	63.89%
Extreme Difference	29%	2.25%	1.46%

the traditional topology for equalization, while the topology proposed in this paper can reduce the extreme difference to 1.46%. It is calculated that the SOC standard deviation of the battery pack before equalization is 9.16. After using the traditional topology and the topology proposed in this paper to equalize, the SOC standard deviation of the battery pack is reduced to 0.73 and 0.48, respectively. From (21), the energy utilization can be improved by about 6% by using the topology proposed in this paper. Thus, it can be seen that the SOC consistency of the battery pack is higher after using the topology proposed in this paper.

The mean value of SOC with error bars is shown in Fig. 10.

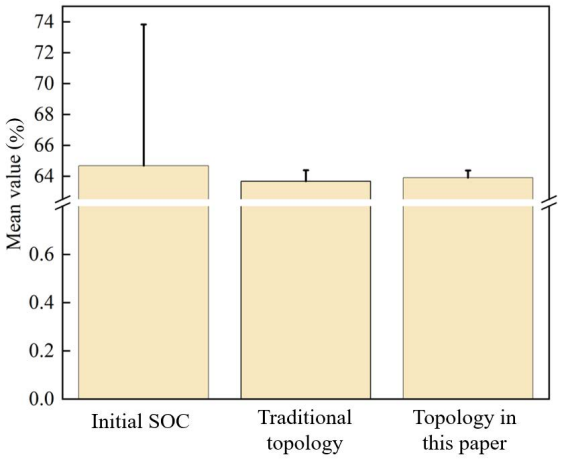

FIGURE 10. SOC mean value diagram with error rod.

The error bar is a line drawn in the direction indicating the magnitude of the measured value with the arithmetic mean of the measured value as the midpoint. It indicates that the measured value falls on the bar with 95% probability. The error bar can reflect the magnitude of the uncertainty of the measured data and the degree of dispersion of the measured data. The shorter the error bar is, the lower the

TABLE 2. Comparison of the composition and performance of the two balanced topologies.

Topology type	Equalization time(s)	Number of components				
		Inductor	Capacitor	MOSFET	Diode	Common switch
Traditional topology	2694	15	0	22	22	0
Proposed topology	2147	8	4	4	8	30

TABLE 3. The results of Charge and discharge equalization.

Number	Charge Equalization		Discharge Equalization	
	Fixed Threshold	C-F Inference	Fixed Threshold	C-F Inference
B1	91.95%	92.56%	37.88%	38.92%
B2	91.70%	92.50%	37.64%	38.74%
B3	91.56%	92.40%	37.42%	38.62%
B4	91.34%	92.24%	37.20%	38.48%
B5	91.10%	92.12%	37.01%	38.31%
B6	90.95%	92.02%	36.76%	38.15%
B7	90.72%	91.85%	36.55%	38.01%
B8	90.54%	91.67%	36.30%	37.88%
B9	90.32%	91.51%	36.03%	37.65%
B10	90.20%	91.40%	35.86%	37.48%
B11	89.94%	91.24%	35.62%	37.32%
B12	89.73%	91.12%	35.40%	37.20%

dispersion of the measured data and the more concentrated the data is.

As can be seen from Fig. 10, the average values of SOC of the battery pack before equalization, after using the traditional topology and after using the topology of this paper have little difference, but after using the topology of this paper for equalization, the error bars are significantly shorter than those of the other two cases, which indicates that after using the topology of this paper for equalization, the SOC distribution of each single cell is more concentrated, the dispersion is lower, and the consistency of the battery pack is higher.

The comparison of the two equalization topologies is shown in Table 2.

From the comparison information in Table 2, it can be seen that the equalization topology proposed in this paper uses double-layer switches instead of switching tubes, and only about one-fifth of MOSFET tubes are needed, although the number of capacitors, diodes, and common switches increases more, it still reduces the hardware cost greatly.

From the above analysis, it is clear that the ZVS QRC equalization topology proposed in this paper can not only reduce turn-on losses and improve energy utilization, but also reduce hardware costs.

B. C-F INFERENCE MODEL VERIFICATION

To better verify the superiority of the C-F inference model proposed in this paper, the charging and discharging experiments and static experiments are conducted in combination with the topology proposed in this paper and compared with the fixed threshold method. The fixed threshold method uses SOC = 3% as the equalization condition. The charge/discharge experiments are performed in the mode of constant current.

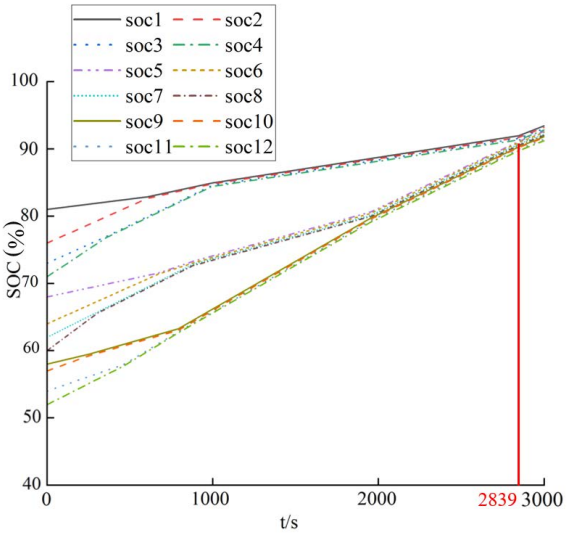

(a) Based on the fixed threshold

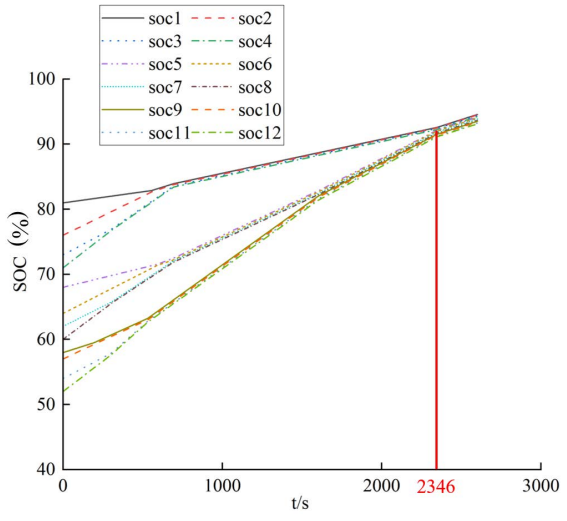

(b) Based on the C-F model inference

FIGURE 11. Charging equalization SOC variation curve.

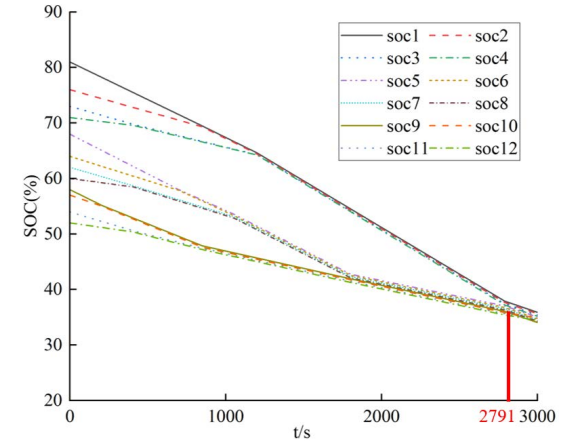

(a) Based on the fixed threshold

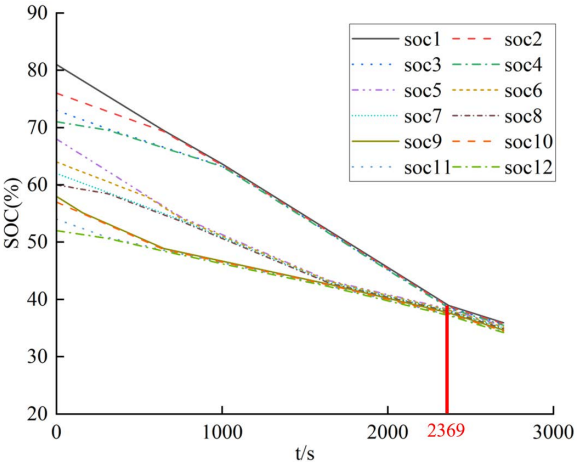

(b) Based on the C-F model inference

FIGURE 12. Discharging equalization SOC variation curve.

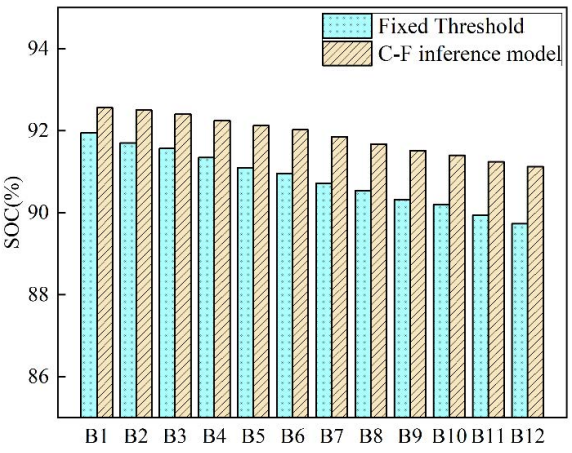

FIGURE 13. SOC distribution of charging equalization.

1) CHARGE AND DISCHARGE EQUALIZATION

The charge-discharge equalization experiments were performed on the battery pack under the same starting conditions. The SOC values of each single cell before and after the charge/discharge equalization experiment are shown in Table 3. The SOC variation curves of each single cell using the fixed threshold method and the C-F inference model for charge/discharge equalization are shown in Fig. 11 and Fig. 12, respectively. The SOC distribution of each single cell after the end of charge/discharge equalization are shown in Fig. 13 and Fig. 14, respectively.

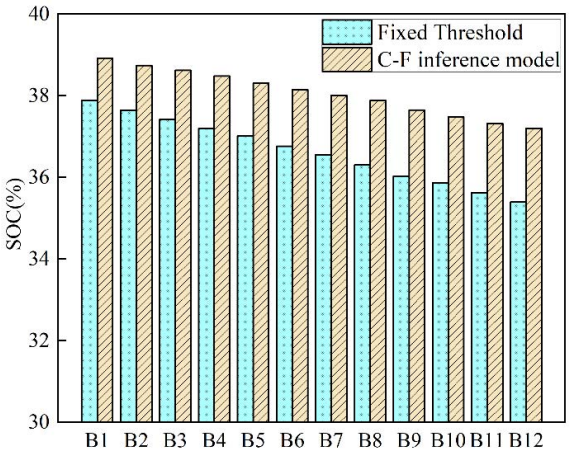

FIGURE 14. SOC distribution of discharging equalization.

From the SOC variation curves in Fig. 11 and Fig. 12, it can be seen that the SOC of the battery pack is increasing under the charging state. It takes about 2839 s to complete the charging equalization using the fixed threshold method, while it only takes 2346 s to complete the equalization by the C-F inference model, saving about 21.01% of the equalization time. In the discharged state, the SOC of the battery pack are decreasing. It takes about 2791 s to complete the charging equalization using the fixed threshold method, while it only takes 2369 s to complete the equalization using the C-F inference model, saving about 17.81% of the equalization time.

From Fig. 13 and Fig. 14, it can be seen that the SOC consistency is higher after equalization with the strategy of the C-F inference model at the end of charge-discharge equalization. According to the data in Table 3, it can be calculated that the extreme difference of SOC after charging equalization is reduced from 29% to 2.22% and 1.44%, respectively, and the SOC standard deviation is reduced from 8.79 to 0.69 and 0.48, respectively; the extreme difference of SOC after discharging equalization is reduced from 29% to 2.48% and 1.72%, respectively, and the SOC standard deviation is reduced from 8.79 to 0.78 and 0.55, respectively. It can be seen that using the C-F inference model for equalization can effectively improve the consistency of the battery pack.

2) STATIC EQUALIZATION

Under the same starting conditions, the battery pack was subjected to static equalization experiments. The variation curves of SOC of each single cell using the fixed threshold method

and C-F inference model for static equalization are shown in Fig. 15. The SOC distribution of each single cell at the end of static equalization are shown in Fig. 16. The SOC values of each single cell before and after the static equalization experiments are shown in Table 4. The comparison of the average values of SOC and equalization time before and after static equalization in the group are shown in Table 5. Where P_1, P_2, and P_3 in Table 5 denote the 1st, 2nd, and 3rd cell groups, respectively.

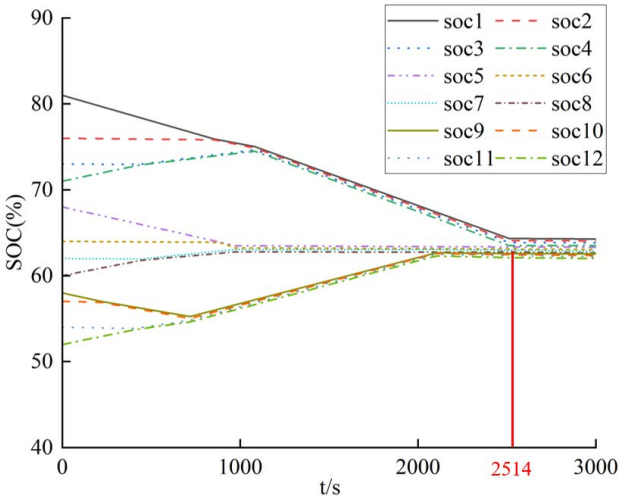

(a) Based on the fixed threshold

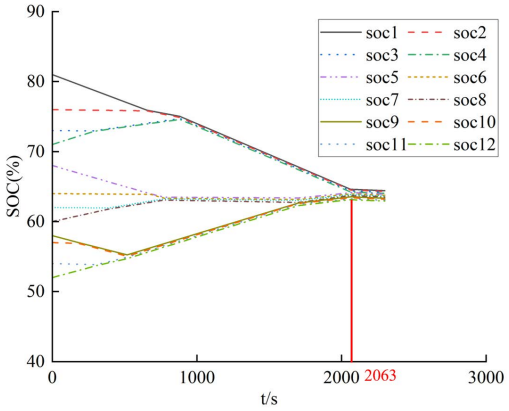

(b) Based on the C-F model inference

FIGURE 15. SOC variation curve of static equilibrium.

From the SOC variation curves in Fig.15, it can be seen that it takes 2514 s to complete the static equilibrium using the fixed-threshold method, while it only takes 2063 s to complete the equilibrium using the C-F inference model, saving about 21.86% of the equilibrium time. It can be seen from Fig. 16 that the SOC consistency is higher after the strategy of using the C-F inference model for equilibration at the end of the static equilibrium.

According to the data in Table 4, it can be calculated that the SOC extreme difference of the battery pack after static equalization is reduced from 29% to 2.46% and 1.48%,

TABLE 4. The results of static equilibrium.

Number	Initial SOC	Fixed Threshold	C-F Inference
B1	81%	64.32%	64.61%
B2	76%	64.08%	64.50%
B3	73%	63.85%	64.39%
B4	71%	63.52%	64.24%
B5	68%	63.35%	64.12%
B6	64%	63.10%	63.96%
B7	62%	62.87%	63.85%
B8	60%	62.66%	63.71%
B9	58%	62.48%	63.54%
B10	57%	62.26%	63.40%
B11	54%	62.02%	63.25%
B12	52%	61.86%	63.13%

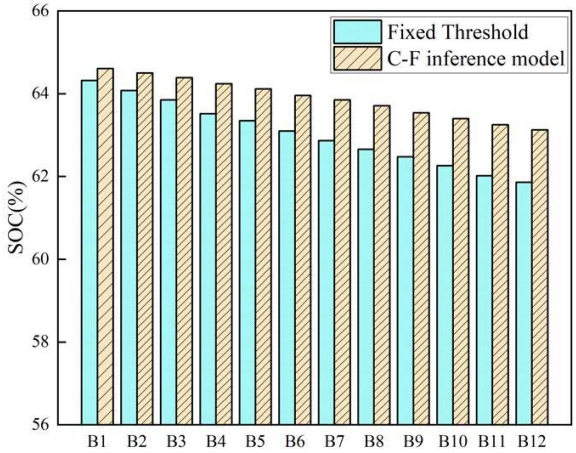

FIGURE 16. Distribution of SOC for each single unit of static equilibrium.

respectively, and the SOC standard deviation is reduced from 8.79 to 0.78 and 0.47, respectively; thus, it can be seen that using the C-F inference model for equalization can effectively improve the consistency of the battery pack. According to (15), it can be calculated that the energy utilization using the C-F inference model for equalization is about 16% higher than that using a fixed threshold for equalization.

From the calculation in Table 5, the SOC standard deviation of the three battery groups before equalization is 8.21, and the SOC standard deviation of the three battery groups at the completion of intra-group equalization is 8.14 and 8.12 for the static equalization using the fixed-threshold method and the C-F inference model, respectively. Combined with the equalization times in Table 5, the equalization time for using the C-F inference model is significantly smaller than the equalization time using the fixed threshold method. This indicates that the C-F inference model can achieve fast equalization and improve the consistency within the group. Combined with the charging and discharging experimental results, it can be further verified that the equalization strategy proposed in this paper can effectively improve the energy utilization and the consistency of the battery pack.

TABLE 5. Comparison of mean values of soc and times before and after static equalization in the group.

Number	Average SOC before equalization	SOC means based on C-F inference	SOC means based on fixed threshold	Time of C-F inference	Time of Fixed Threshold
P1	75.25%	74.79%	74.75%	883s	1109s
P2	63.50%	63.28%	63.13%	746s	974s
P3	55.25%	54.98%	54.92%	552s	718s

V. CONCLUSION

In this paper, a two-stage balanced topology based on ZVS QRC is proposed to solve the problem of long equalization time and low energy utilization of series lithium-ion battery packs. ZVS QRCs are adopted in both intra-group and inter-group. This topology can effectively solve the switching loss problem of the battery pack during equalization by introducing a quasi-resonant circuit, which can effectively improve the energy utilization of the battery pack. The simulation results show that the proposed topology improves the energy utilization by about 6% and reduces the equalization time by about 25.48% compared with the traditional Buck-Boost group equalization topology. With SOC as the equalization target, a control strategy based on the C-F inference model is proposed in this paper. To verify the feasibility and superiority of the strategy, comparison experiments are conducted with the fixed-threshold method under static and charge-discharge conditions. Simulation results show that under the same equalization conditions, the strategy based on C-F inference model proposed in this paper shortens the equalization time by about 20%, improves the energy utilization by about 16%, and effectively improves the consistency of the series-connected battery pack.

REFERENCES

[1] L. Chen, Y.-N. Nie, H. Yu, and W.-Q. Tao, "Study on the mechanism of destruction triggering of membrane electrode assembly of hydrogen fuel cell," *Int. J. Heat Mass Transf.*, vol. 159, Oct. 2020, Art. no. 120144.

[2] L. Lu, X. Han, J. Li, J. Hua, and M. Ouyang, "A review on the key issues for lithium-ion battery management in electric vehicles," *J. Power Sources*, vol. 226, pp. 272–288, Mar. 2013.

[3] T. Wu, Y. Qi, L. Liao, F. Ji, and H. Chen, "Research on equalization strategy of lithium-ion batteries based on fuzzy logic control," *J. Energy Storage*, vol. 40, Aug. 2021, Art. no. 102722.

[4] X. Hu, C. Zou, C. Zhang, and Y. Li, "Technological developments in batteries: A survey of principal roles, types, and management needs," *IEEE Power Energy Mag.*, vol. 15, no. 5, pp. 20–31, Sep. 2017.

[5] X. Lai, D. Qiao, Y. Zheng, M. Ouyang, X. Han, and L. Zhou, "A rapid screening and regrouping approach based on neural networks for large-scale retired lithium-ion cells in second-use applications," *J. Cleaner Prod.*, vol. 213, pp. 776–791, Mar. 2019.

[6] S. M. Lukic, J. Cao, R. C. Bansal, F. Rodriguez, and A. Emadi, "Energy storage systems for automotive applications," *IEEE Trans. Ind. Electron.*, vol. 55, no. 6, pp. 2258–2267, Jun. 2008.

[7] M.-Y. Kim, J.-H. Kim, and G.-W. Moon, "Center-cell concentration structure of a cell-to-cell balancing circuit with a reduced number of switches," *IEEE Trans. Power Electron.*, vol. 29, no. 10, pp. 5285–5297, Oct. 2014.

[8] Y. Shang, B. Xia, C. Zhang, N. Cui, J. Yang, and C. C. Mi, "An automatic equalizer based on forward-flyback converter for series-connected battery strings," *IEEE Trans. Ind. Electron.*, vol. 64, no. 7, pp. 5380–5391, Jul. 2017.

[9] L. Liao and H. Chen, "Research on two-stage equalization strategy based on fuzzy logic control for lithium-ion battery packs," *J. Energy Storage*, vol. 50, Jun. 2022, Art. no. 104321.

[10] Z. B. Omariba, L. Zhang, and D. Sun, "Review of battery cell balancing methodologies for optimizing battery pack performance in electric vehicles," *IEEE Access*, vol. 7, pp. 129335–129352, 2019.

[11] M. Gao, J. Qu, H. Lan, Q. Wu, H. Lin, Z. Dong, and W. Zhang, "An active and passive hybrid battery equalization strategy used in group and between groups," *Electronics*, vol. 9, no. 10, p. 1744, Oct. 2020.

[12] X. Ding, D. Zhang, J. Cheng, B. Wang, Y. Chai, Z. Zhao, R. Xiong, and P. C. K. Luk, "A novel active equalization topology for series-connected lithium-ion battery packs," *IEEE Trans. Ind. Appl.*, vol. 56, no. 6, pp. 6892–6903, Dec. 2020.

[13] S. Wang, S. Yang, W. Yang, and Y. Wang, "A new kind of balancing circuit with multiple equalization modes for serially connected battery pack," *IEEE Trans. Ind. Electron.*, vol. 68, no. 3, pp. 2142–2150, Mar. 2021.

[14] Y. Li, J. Xu, X. Mei, and J. Wang, "A unitized multiwinding transformer-based equalization method for series-connected battery strings," *IEEE Trans. Power Electron.*, vol. 34, no. 12, pp. 11981–11989, Dec. 2019.

[15] R. K. Vardhan, T. Selvathai, R. Reginald, P. Sivakumar, and S. Sundaresh, "Modeling of single inductor based battery balancing circuit for hybrid electric vehicles," in *Proc. 43rd Annu. Conf. IEEE Ind. Electron. Soc. (IECON)*, Beijing, China, Oct. 2017, pp. 2293–2298.

[16] Z. Fan, M. Yan, D. Peng, M. Chen, and C. Hong, "Non-dissipative equalization with voltage-difference based on FPGA for lithium-ion battery," in *Proc. Chin. Control Decis. Conf. (CCDC)*, Shenyang, China, Jun. 2018, pp. 1132–1137.

[17] Y. Ma, P. Duan, Y. Sun, and H. Chen, "Equalization of lithium-ion battery pack based on fuzzy logic control in electric vehicle," *IEEE Trans. Ind. Electron.*, vol. 65, no. 8, pp. 6762–6771, Aug. 2018.

[18] I. Zeltser, M. Evzelman, A. Kuperman, and M. M. Peretz, "Zero current switching resonant converter based parallel balancing of serially connected batteries string," *IEEE Trans. Ind. Appl.*, vol. 55, no. 6, pp. 7452–7460, Nov. 2019.

[19] K. M. Lee, Y. C. Chung, C. H. Sung, and B. Kang, "Active cell balancing of li-ion batteries using LC series resonant circuit," *IEEE Trans. Ind. Electron.*, vol. 62, no. 9, pp. 5491–5501, Sep. 2015.

[20] Y. Shang, B. Xia, C. Zhang, N. Cui, J. Yang, and C. Mi, "A modularization method for battery equalizers using multiwinding transformers," *IEEE Trans. Veh. Technol.*, vol. 66, no. 10, pp. 8710–8722, Oct. 2017.

[21] M. W. Einhorn, W. Guertlschmid, T. Blochberger, R. Kumpusch, R. Permann, F. V. Conte, C. Kral, and J. Fleig, "A current equalization method for serially connected battery cells using a single power converter for each cell," *IEEE Trans. Veh. Technol.*, vol. 60, no. 9, pp. 4227–4237, Nov. 2011.

[22] L. Song, T. Liang, L. Lu, and M. Ouyang, "Lithium-ion battery pack equalization based on charging voltage curves," *Int. J. Electr. Power Energy Syst.*, vol. 115, Feb. 2020, Art. no. 105516.

[23] S.-W. Lee, K.-M. Lee, Y.-G. Choi, and B. Kang, "Modularized design of active charge equalizer for Li-ion battery pack," *IEEE Trans. Ind. Electron.*, vol. 65, no. 11, pp. 8697–8706, Nov. 2018.

[24] Y. Zheng, M. Ouyang, L. Lu, J. Li, X. Han, and L. Xu, "On-line equalization for lithium-ion battery packs based on charging cell voltages: Part 1. Equalization based on remaining charging capacity estimation," *J. Power Sources*, vol. 247, pp. 676–686, Feb. 2014.

[25] X. Cui, W. Shen, Y. Zhang, C. Hu, and J. Zheng, "Novel active $LiFePO_4$ battery balancing method based on chargeable and dischargeable capacity," *Comput. Chem. Eng.*, vol. 97, pp. 27–35, Feb. 2017.

[26] Y.-S. Lee and M.-W. Cheng, "Intelligent control battery equalization for series connected lithium-ion battery strings," *IEEE Trans. Ind. Electron.*, vol. 52, no. 5, pp. 1297–1307, Oct. 2005.

[27] Y. Lin, X. Xu, F. Wang, and Q. Xu, "Active equalization control strategy of Li-ion battery based on state of charge estimation of an electrochemical-thermal coupling model," *Int. J. Energy Res.*, vol. 44, no. 5, pp. 3778–3789, Apr. 2020.

[28] M. Kamel, V. Sankaranarayanan, R. Zane, and D. Maksimovic, "State-of-Charge balancing with parallel and series output connected battery power modules," *IEEE Trans. Power Electron.*, vol. 37, no. 6, pp. 6669–6677, Jun. 2022.

LI LIAO was born in Hubei, China, in 1979. He received the Ph.D. degree in water conservancy and hydropower engineering from the Huazhong University of Science and Technology, China, in 2013. He is an Associate Professor with the Hubei University of Technology. He has published over 20 journal articles and conference papers. His research interests include energy storage technology and electric vehicle battery management systems.

HENG CHEN was born in Hubei, China, in 1997. He received the B.S. degree in electrical engineering and automation from Wuchang Shouyi University, Wuhan, China, in 2019. He is currently pursuing the M.S. degree with the Hubei University of Technology, Wuhan. His current research interests include electric vehicle battery management systems and battery equalization.

SHU SUN was born in Hubei, China, in 1997. He received the B.S. degree in automation from the Hubei University of Technology, Wuhan, China, in 2020. He is currently pursuing the M.S. degree with the Hubei University of Technology, Wuhan. His current research interests include electric vehicle battery management systems and battery equalization.

HONGGUANG LI was born in Henan, China, in 1999. He received the B.S. degree in electrical engineering and automation from the Henan University of Technology, Zhengzhou, China, in 2021. He is currently pursuing the M.S. degree with the Hubei University of Technology, Wuhan, China. His current research interests include electric vehicle battery management systems and battery equalization.

JIUCHUN JIANG (Senior Member, IEEE) was born in Jilin, China. He received the B.S. degree in electrical engineering and the Ph.D. degree in power system automation from Northern Jiaotong University, Beijing, China, in 1993 and 1999, respectively. He was a Professor at the School of Electrical Engineering, Beijing Jiaotong University, Beijing, until 2018. He is currently with the Hubei University of Technology, Wuhan. His research interests include battery application technology, electric car charging stations, and microgrid technology. He was a recipient of the National Science and Technology Progress 2nd Award for his work on electric vehicle (EV) bus systems, and the Beijing Science and Technology Progress 2nd Award for his work on EV charging systems.

TIEZHOU WU received the B.S. degree in radio and information engineering from Wuhan University, China, in 1988, and the M.S. degree in engineering from Naval Engineering University, China, in 2003, and the Ph.D. degree in systems analysis and integration from the Huazhong University of Science and Technology, China, in 2010. He is currently the Executive Vice President of the Solar Energy Research Institute, Hubei University of Technology, and the Collaborative Innovation Center, Hubei, for efficient utilization of solar energy, and the Director of the Key Laboratory of Solar Power Generation and Energy Storage Operation Control. His research interests include energy storage technology, photovoltaic power generation technology, system analysis, and integration.